ORIGINAL ARTICLE

lajss.org© Latin American Journal of Solids and Structures

www.lajss.org

ON AN INTEGRATED DYNAMIC CHARACTERIZATION OF VISCOELASTIC MATERIALS BY FRACTIONAL DERIVATIVE AND GHM MODELS

Wagner Barbosa de Medeiros Júnior[a*]

Cíntia Teixeira Préve[a]

Fernanda Oliveira Balbino[a]

Thatiane Alves da Silva[a]

Eduardo Márcio de Oliveira Lopes[a]

[a] Departamento de Engenharia Mecânica, Universidade Federal do Paraná, R. Cel. Francisco H. dos Santos, s/n; 81530-900, Curitiba, PR, Brasil. E-mail: wagnerbmj@gmail.com, cintiapreve@gmail.com, ferbalbino@yahoo.com.br, thatianec95@gmail.com, eduardo_lopes@ufpr.br

*Corresponding author

http://dx.doi.org/10.1590/1679-78254983

Abstract

The passive vibration control of mechanical systems under unwanted vibrations can be accomplished in a very effective way by using devices incorporating viscoelastic materials. The design of such devices requires a broad knowledge of the dynamic properties of the employed viscoelastic material, usually supplied by adequate mathematical models. Among the available mathematical models, the fractional derivative (FD) model and the Golla-Hughes-McTavish (GHM) model, along with either the Williams-Landel-Ferry (WLF) equation or the Arrhenius equation, are now very prominent. The current work investigates the use of these models in a wide and integrated dynamic characterization of a typical and thermorheologically simple viscoelastic material. It focuses on experimental data collected from 0.1 to 100 Hz and –40 °C to 50 °C, which are simultaneously manipulated to raise both the frequency and the temperature dependencies of the material. In fitting the models, a hybrid approach - combining techniques of genetic algorithms and nonlinear optimization - is adopted. The ensuing results are evaluated by means of objective function values, comparative experimental-predicted data plots, and the Akaike's Information Criterion (AIC). It is shown that the four-parameter fractional derivative model presents excellent curve fitting results. As for the GHM model, its modified version is the most adequate, although a higher number of terms is required for a satisfactory goodness-of-fit. None the less the fractional derivative model stands out.

Keywords

Dynamic Properties, Fractional Derivative Model, GHM Model, Vibration Control, Viscoelastic Materials.

1 INTRODUCTION

Effective actions of vibration control with viscoelastic devices generally require a previous and wide knowledge of the dynamic behavior of the employed viscoelastic materials, particularly their so-called dynamic properties: the dynamic elasticity modulus and the corresponding loss factor. Among other factors, these properties are dependent on frequency and temperature, and this dependence can be quite pronounced (Nashif et al., 1985).

A usual and established way of describing the dynamic behavior of viscoelastic materials, combining the previously mentioned properties, is the representation by complex moduli (Snowdon, 1968). In a complex modulus description,

Received: March 13, 2018. In Revised Form: December 09, 2018. Accepted: January 03, 2019. Available online: January 04, 2019.
http://dx.doi.org/10.1590/1679-78254983

(cc) BY

the real part contains the elastic characteristics of the material, whereas the imaginary part supplies its dissipative characteristics.

The complex modulus representation is usually constructed in two stages: one is experimental, and the other is analytical and numerical. In the latter, a mathematical model is conveniently fitted to experimental data collected in the former. For a complete description of its dynamic behavior, a viscoelastic material (VEM) must be tested over broad ranges of frequency and temperature.

Two mathematical models that represent the dynamic behavior of viscoelastic materials (VEMs) have been objects of primary interest in the present work: the fractional - or generalized - derivative (FD) model (Bagley and Torvik, 1983; Bagley and Torvik, 1986; Pritz, 1996; Espíndola et al., 2005) and the Golla-Hughes-McTavish (GHM) model (Golla and Hughes, 1985; Gibson and McTavish, 1995; Friswell et al., 1997; Martin and Inman, 2013).

Both models have been extensively used in the dynamic behavior analysis of mechanical systems with viscoelastic inserts, particularly regarding vibration control. For the FD model, renowned for its ability to represent the behavior of many VEMs of concern with a small number of parameters, the papers by Espíndola et al. (2010), Ribeiro et al. (2015), Sun and Chen (2015), Zhu et al. (2015), and Katsikadelis (2015) are illustrative examples. As for the GHM model, its adequacy to time domain and finite element descriptions is well shown in Barbosa and Farage (2008), Kattimani and Ray (2014, 2015), Zghal et al. (2015), and Cunha-Filho et al. (2016).

The present paper is specifically concerned with two of those models, namely, the four-parameter fractional derivative model (Bagley and Torvik, 1986; Lopes, 1998) and the modified GHM (MGHM) model (Martin, 2011), which are presented in the following sections aiming at a broad and integrated dynamic characterization of a commercial VEM, namely, ISODAMP C-1002, manufactured by EAR – Aearo Technologies LLC (3M Group). This is a typical, thermorheologically simple viscoelastic material, already well investigated (Jones, 1992). It considers experimental data collected from 0.1 to 100 Hz and –40 °C to 50 °C, which are simultaneously manipulated to raise both frequency and temperature dependencies. The experimental procedure is also described in a coming section.

The current investigation builds on a previous work carried out by some of the authors (Medeiros Jr et al., 2011). At that stage, using a different viscoelastic material, the four-parameter FD model (Bagley and Torvik, 1986; Pritz, 1996), also known as the fractional Zener model (Mainardi, 2010), was compared to two current versions of the GHM model, namely, the standard (SGHM) and the alternative (AGHM) models, with and without additional terms. The R^2 index was then used in the analysis of the corresponding results.

At present, a more comprehensive picture is offered taking into account the modified (latest) GHM (MGHM) model, with and without additional terms, besides exploring a more informative approach of model comparison, the Akaike's Information Criterion (AIC), which was unknown to the authors at that time. As it will be observed, the pertinent analysis is even more revealing and incisive, providing new insights on the subject.

2 DYNAMIC CHARACTERIZATION

All viscoelastic solids have elastic and dissipative properties. Such properties may be well represented, in the linear region, by complex functions. These complex functions are called 'complex moduli of elasticity' (Snowdon, 1968; Pritz, 1998). Thus, there are the complex bulk, shear and Young moduli, and also the complex Poisson's ratio.

The complex Young modulus $\bar{E}$ [Pa] represents the dynamic relation between the uniaxial longitudinal stress σ and the associated uniaxial longitudinal deformation ε. Among other factors, it is clearly dependent on frequency and temperature (Nashif et al., 1985). Therefore, it can be expressed as

$$\frac{\sigma}{\varepsilon} = \overline{E}(\Omega, T) = E_R(\Omega, T) + iE_I(\Omega, T) \tag{1}$$

where Ω is frequency [rad/s], T is temperature [K], E_R is the real Young modulus [Pa], associated with the stored energy, and E_I is the imaginary Young modulus [Pa], associated with the dissipated energy, and i is the imaginary unit.

Defining the loss factor η_E as the ratio of E_I to E_R (it is, therefore, dimensionless), the modulus can $\bar{E}$ be rewritten as

$$\overline{E}(\Omega, T) = E_R(\Omega, T)[1 + i\eta_E(\Omega, T)] \tag{2}$$

There is a similar expression for the complex shear modulus $\bar{G}$ [Pa], which is

$$\overline{G}(\Omega,T) = G_R(\Omega,T)[1+in_G(\Omega,T)] \tag{3}$$

Experimental data concerning the so-called dynamic properties E_R and η_E is obtained from tests in a range of frequencies and temperatures of interest, generating curves like those in Figure 1.

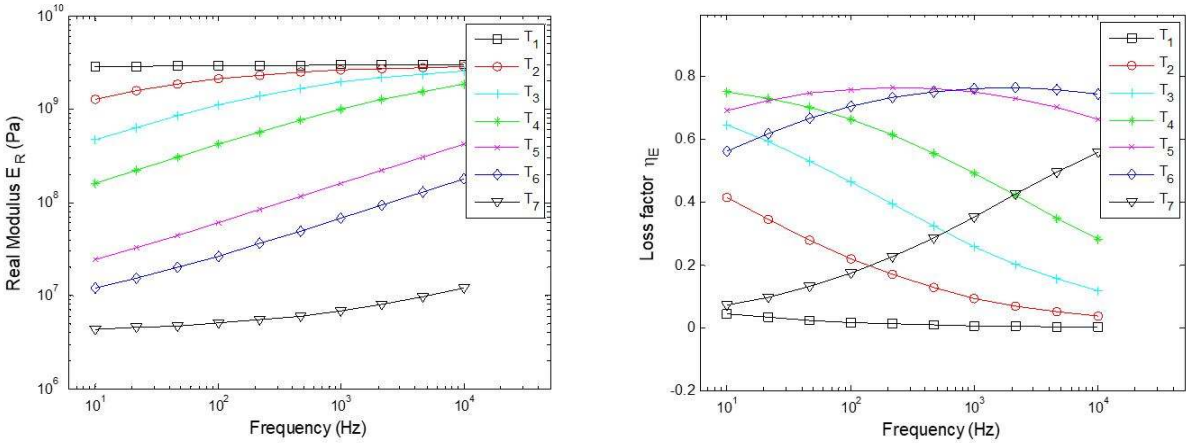

Figure 1: Experimental plots of dynamic properties.

The experimental data can be assembled by the frequency-temperature superposition principle (Nashif et al., 1985). This principle states that the various curves of dynamic properties obtained over a frequency range in distinct temperatures (Fig. 1) can be superimposed, in a temperature of reference, by means of shifts in frequency. Thus, as seen in Figure 2, single master curves are formed in a standardized plot called reduced frequency nomogram (Jones, 2001).

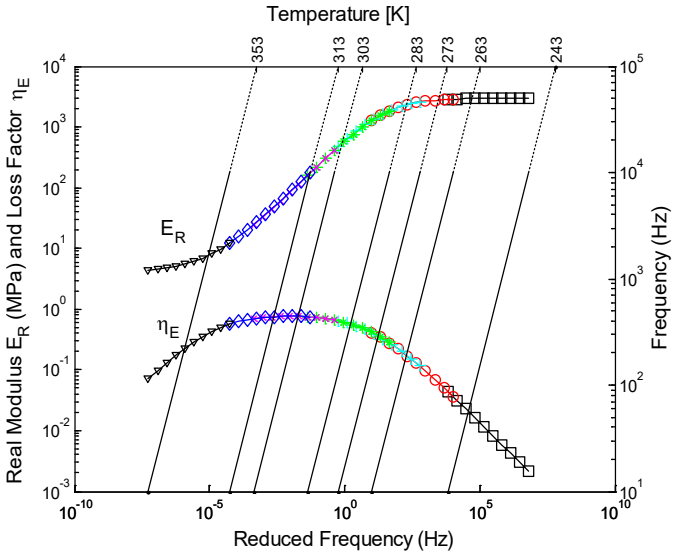

Figure 2: A reduced frequency nomogram.

In mathematical terms, the superposition principle establishes that

$$E_R(\Omega_r) = (T_0\rho_0/T\rho)\, E_R(\Omega,T) \tag{4}$$

and

$$n_E(\Omega_r) = n_E(\Omega,T) \tag{5}$$

where Ω_r is the so-called reduced frequency [rad/s], T_0 is the temperature of reference [K], ρ is the material density [kg/m^3], and ρ_0 is the material density at the reference temperature [kg/m^3].

The above expressions show that, except for the factor $(T_0\rho_0/T\rho)$ (usually negligible), the values of the dynamic properties at a frequency Ω and a temperature *T* are equal to the values of the same properties at a reduced frequency Ω_r and the reference temperature T_0.

The reduced frequency Ω_r is given by

$$\Omega_r = \alpha_T(T)\Omega \tag{6}$$

where $\alpha_T(T)$, which is dimensionless, is known as the 'shift factor'. The shift factor, as the name implies, accounts for the shifts in frequency required to take the curves of dynamic properties from their specific measurement temperatures to the reference temperature.

The shift factor can be modeled in several ways. The most employed models are: the WLF (Williams-Landel-Ferry) equation, in which

$$log_{10}\alpha_T(T) = \frac{-\theta_1(T-T_0)}{\theta_2+T-T_0} \tag{7}$$

where θ_1 and θ_2 are specific material parameters to be raised from experimental data; and the Arrhenius equation, in which

$$log_{10}\alpha_T(T) = \frac{T_A}{T} - \frac{T_A}{T_0} \tag{8}$$

where T_A is the so-called 'activation temperature' [K], also a material parameter. It is considered that, from a practical point of view, any of these equations can be employed (Mead, 2000).

For the sake of usability, mathematical models can be fitted to the master curves presented in a reduced frequency nomogram. Two of those models, the fractional derivative model and the GHM model, stand out.

3 FRACTIONAL DERIVATIVE (FD) MODEL

The one-dimensional fractional derivative constitutive equation at a given temperature is (Bagley, 1979; Pritz, 2003)

$$\sigma(t) + \sum_{m=1}^{M} b_m D^{\beta_m}[\sigma(t)] = E_0\mathcal{E}(t) + \sum_{n=1}^{N} E_n D^{\alpha_n}[\mathcal{E}(t)] \tag{9}$$

where b_m $\left[s^{\beta_m}\right]$, β_m (dimensionless), E_0 [Pa], E_n [Pa], and α_n (dimensionless) are material parameters, with *m* from 1 to *M* and *n* from 1 to *N*. As to D^{β_m} and D^{α_n}, they are fractional order derivatives, the Riemann-Liouville (RL) definition of which is

$$D^{\alpha}[x(t)] = \frac{1}{\Gamma(1-\alpha)}\frac{d}{dt}\int_0^t \frac{x(\tau)}{(t-\tau)^{\alpha}}d\tau \tag{10}$$

where α is the fractional derivative order, such that $0 < \alpha < 1$, Γ is the gamma function, and τ is an integration variable (Bagley and Torvik, 1983; Nashif et al., 1985).

As pointed out by Bagley and Torvik (1983, 1986) and Pritz (2003), the fractional calculus approach has been shown to be an efficient and robust tool for describing the dynamic behavior of real viscoelastic materials, particularly elastomers used in noise and vibration control designs. That has also been observed by Lopes et al. (2004), Espíndola et al. (2005) and Medeiros Jr (2010), in instances particularly familiar to the current authors.

Similarly to integer order derivatives, it can be shown that the Fourier transform (denoted by F) of the above defined fractional order derivative of a certain function f(t) is given by

$$\mathfrak{F}\{D^{\alpha}[f(t)]\} = (i\Omega)^{\alpha}\mathfrak{F}\{f(t)\} \tag{11}$$

Considering Eq. (9) with only four material parameters, it follows that

$$\sigma(t) + b_1 D^{\beta_1}[\sigma(t)] = E_0 \mathcal{E}(t) + E_1 D^{\beta_1}[\mathcal{E}(t)] \tag{12}$$

in which $\alpha_1 = \beta_1$, based on thermodynamic considerations (Bagley and Torvik, 1986). The preceding equation can be represented by an arrangement of mechanical elements as shown in Cinielo et al. (2017).

Fourier transforming both sides of Eq. (12) gives

$$\overline{E}(\Omega) = \frac{\overline{\sigma}(\Omega)}{\overline{\varepsilon}(\Omega)} = \frac{E_0 + E_1 (i\Omega)^{\beta_1}}{1 + b_1 (i\Omega)^{\beta_1}} \tag{13}$$

An alternative expression for $\overline{E}(\Omega)$ is

$$\overline{E}(\Omega) = \frac{E_0 + E_\infty b (i\Omega)^{\beta}}{1 + b (i\Omega)^{\beta}} \tag{14}$$

where $\beta_1 = \beta$ and $b_1 = b$, for simplicity, and $E_1 = E_\infty b$ for convenience. This expression is known as the four-parameter fractional derivative model for the complex Young modulus.

The inclusion of temperature dependence in the above equation, via the shift factor α_T, gives

$$\overline{E}(\Omega, T) = \frac{E_0 + E_\infty b\, [i\alpha_T(T)\Omega]^{\beta}}{1 + b\, [i\alpha_T(T)\Omega]^{\beta}} \tag{15}$$

4 GHM MODEL

4.1 Standard GHM (SGHM) model

The standard (original) GHM model can be introduced as follows: consider a simple structure under longitudinal stress and assume the existence of a material relaxation function *E(t)* [Pa] given by

$$E(t) = E_C \mu(t) + \mathrm{H(t)} \tag{16}$$

where $\mu(t)$ is a unit step function, $E_C = \lim_{t \to \infty} E(t)$ is the elastic equilibrium modulus of the material [Pa], and *H(t)* is the time dependent relaxation function [Pa] (Moschen, 2006; Christensen, 1982).

It is known that the resultant stress for a sudden deformation applied at t = 0 can be written as either

$$\sigma(t) = \int_0^t E(t-\phi) \frac{d}{d\phi} [\varepsilon(\phi)] d\phi \tag{17}$$

or, given Eq. (16),

$$\sigma(t) = \int_0^t [E_c \mu(t-\phi) + H(t-\phi)] \frac{d}{d\phi} [\varepsilon(\phi)] d\phi \tag{18}$$

Besides linearity and causality, it is also assumed above that the material is relaxed.

As the GHM model is developed in the Laplace domain, it is worth noting that, in the current context, the Laplace transform (denoted by L) of a function f(t) can be given by (Papoulis, 1962)

$$\mathcal{L}\{f(t)\} = \int_0^\infty f(t) e^{-st} dt = \lim_{y \to \infty} \left[\int_0^y f(t) e^{-st} dt \right] \tag{19}$$

Thus, Laplace transforming Eqs. (17) and (18) provides, respectively,

$$\overline{\sigma}(s) = s \overline{E}_s(s) \overline{\varepsilon}(s) \tag{20}$$

and

$$\overline{\sigma}(s) = \left[E_c + s\overline{H}(s)\right]\overline{\varepsilon}(s) \tag{21}$$

From Eqs (20) and (21), it follows that

$$s\overline{E}_s(s) = \left[E_c + s\overline{H}(s)\right] \tag{22}$$

For the sake of simplicity, the terms $s\overline{E}_s(s)$ and $s\overline{H}(s)$, which are the complex Young modulus and the complex dissipation function in the Laplace domain, can be denoted as $\overline{E}(s)$ and $\overline{h}(s)$, in such a way that

$$\overline{E}(s) = \left[E_c + \overline{h}(s)\right] \tag{23}$$

The complex dissipation function $\overline{h}(s)$ has several forms and, therefore, it must be chosen by the analyst (Golla and Hughes, 1985; Barbosa, 2000). Usually, a function obtained from the Biot series (Biot, 1955) is employed in the following form

$$\overline{h}(s) = \sum_{k=1}^{n} \frac{a_k s}{s+b_k} \tag{24}$$

This series is truncated to the second term, with $b_2 > b_1 > b_0$, to produce what is called a 'dissipation pole pair' (Golla and Hughes, 1985), commonly written as

$$\overline{h}(s) = \frac{\hat{\alpha}s^2+\hat{\gamma}s}{s^2+\hat{\beta}s+\hat{\delta}} \tag{25}$$

where $\hat{\alpha} = a_1 + a_2\ [Pa]$, $\hat{\gamma} = a_1 b_2 + a_2 b_1\ [Pa.s^{-1}]$, $\hat{\beta} = b_1 + b_2\ [s^{-1}]$, and $\hat{\delta} = b_1 b_2\ [s^{-2}]$, with $\left(\hat{\alpha}, \hat{\gamma}, \hat{\beta}, \hat{\delta}\right) > 0$.

Applying the restriction $\hat{\gamma} = \hat{\alpha}\hat{\beta}$, established by Golla and Hughes (1985) when the modeling of vibrating systems is considered, the expression for the complex Young modulus in the Laplace domain is obtained, which is

$$\overline{E}(\Omega) = E_c + \frac{\hat{\alpha}(s^2+\hat{\beta}s)}{s^2+\hat{\beta}s+\hat{\delta}} \tag{26}$$

Assuming that the Fourier transform can be treated as a special case of the Laplace transform, with $s = i\Omega$ (see Papoulis, 1962), the complex Young modulus in the frequency domain, for a given temperature, can be written, from Eq. (26), as

$$\overline{E}(\Omega, T) = E_C + \frac{\hat{\alpha}(-\Omega^2+i\hat{\beta}\Omega)}{-\Omega^2+i\hat{\beta}\Omega+\hat{\delta}} \tag{27}$$

Equation (27) is the standard GHM counterpart of Eq. (14), which describes the complex Young modulus by the use of fractional calculus.

Including the temperature dependence in Eq. (27), as done in the previous section, gives

$$\overline{E}(\Omega, T) = E_C + \frac{\hat{\alpha}\{-[\alpha_T(T)\Omega]^2+i\hat{\beta}\alpha_T(T)\Omega\}}{-[\alpha_T(T)\Omega]^2+i\hat{\beta}\alpha_T(T)\Omega+\hat{\delta}} \tag{28}$$

4.2 Additional GHM Terms

In order to achieve satisfactory curve fitting results for the GHM model (regarding experimental data), the strategy of expanding the model by increasing the number of dissipation pole pairs in the dissipation function $\overline{h}(s)$ is commonly employed. Each new pair adds its specific contribution to the behavior of the dynamic property curves.

Thus, the complex Young modulus in Laplace domain is expressed by

$$\overline{E}(\Omega) = E_C + \sum_{k=1}^{n} \frac{\hat{\alpha}_k(-\Omega^2 + i\hat{\beta}_k\Omega)}{-\Omega^2 + i\hat{\beta}_k\Omega + \hat{\delta}_k} \tag{29}$$

where k is the number of dissipation pole pairs or, simply, GHM terms.

In the frequency domain, it gives

$$\overline{E}(s) = E_C + \sum_{k=1}^{n} \frac{\hat{\alpha}_k(s^2 + \hat{\beta}_k s)}{s^2 + \hat{\beta}_k s + \hat{\delta}_k} \tag{30}$$

However, as new GHM terms are added, new problems also appear, since the terms are not orthogonal functions, and it is very difficult to obtain initial estimates for the additional parameters. To circumvent these problems, Gibson and McTavish (1995) introduced a parameter reduction, relating parameters $\hat{\beta}$ and $\hat{\delta}$ by

$$u\hat{\beta}_k = \sqrt{\hat{\delta}_k} \tag{31}$$

where *0 < u < 1*.

Also, the values of $\hat{\beta}_k$ are restricted to the geometric series

$$\hat{\beta}_k = r^{k-1}\hat{\beta}_1 \tag{32}$$

where *r* is the geometric growth ratio of $\hat{\beta}$.

Given the modifications introduced by Eqs (31) and (32), instead of (3k+1) parameters, the expanded GHM model contains (k+4) parameters. It should be stressed that the above discussion refers to a condition of constant temperature. The temperature dependence can be introduced, as explained in a previous section.

4.3 Alternative GHM (AGHM) Model

An alternative form of the GHM model was presented by Friswell et al. (1997), in which the restriction $\hat{\gamma} = \hat{\alpha}\hat{\beta}$, established by Golla and Hughes (1985) and pointed out before, was no longer necessary. Deriving again the expression for the complex Young modulus in the frequency domain, without the above restriction, it follows that (see Eqs. (25) and (26))

$$\overline{E}(\Omega) = E_C + \frac{-\hat{\alpha}\Omega^2 + i\hat{\gamma}\Omega}{-\Omega^2 + i\hat{\beta}\Omega + \hat{\delta}} \tag{33}$$

Rearranging terms in Eq. (33) and introducing new parameters produces

$$\overline{E}(\Omega) = E_\infty + \frac{i\hat{\theta}\Omega + \hat{\mu}}{-\Omega^2 + i\hat{\beta}\Omega + \hat{\delta}} \tag{34}$$

where $E_\infty = E_C + \hat{\alpha}\ [Pa]$, $\hat{\theta} = \hat{\gamma} - \hat{\alpha}\hat{\beta}\ [Pa.s^{-1}]$, and $\hat{\mu} = -\hat{\alpha}\hat{\delta}\ [Pa.s^{-2}]$.

This form can also be expanded to contain additional terms, in a similar fashion to that previously presented for Eq. (30). As for the temperature dependence, it can be also included in Eq. (34) to provide

$$\overline{E}(\Omega, T) = E_\infty + \frac{i\hat{\theta}\alpha_T(T)\Omega + \hat{\mu}}{-[\alpha_T(T)\Omega]^2 + i\hat{\beta}\alpha_T(T)\Omega + \hat{\delta}} \tag{35}$$

4.4 Modified GHM (MGHM) Model

A modified GHM model was originally introduced by Martin (2011) and further reported by Martin and Inman (2013), resorting again to the restriction $\hat{\gamma} = \hat{\alpha}\hat{\beta}$ and multiplying parameter $\hat{\beta}$ by an auxiliary parameter $\hat{\psi}$, either in the numerator or the denominator of Eq. (27), to create a novel parameter $\hat{\phi} = \hat{\psi}\hat{\beta}$. Choosing to introduce this parameter into the numerator, the result is

$$\overline{E}(\Omega) = E_C + \frac{\widehat{\alpha}(-\Omega^2 + i\widehat{\phi}\Omega)}{-\Omega^2 + i\widehat{\beta}\Omega + \widehat{\delta}} \tag{36}$$

As before, the MGHM model can also be expanded to contain additional terms, as shown in Eq. (30). Regarding the temperature dependence, it can be included in Eq. (36) to provide

$$\overline{E}(\Omega, T) = E_C + \frac{\widehat{\alpha}\{-[\alpha_T(T)\Omega]^2 + i\widehat{\phi}\alpha_T(T)\Omega\}}{-[\alpha_T(T)\Omega]^2 + i\widehat{\beta}\alpha_T(T)\Omega + \widehat{\delta}} \tag{37}$$

As it is of concern to the current paper, the complex Young modulus equation for the MGHM model is presented below including the temperature dependence and additional terms. It is

$$\overline{E}(\Omega, T) = E_C + \sum_{k=1}^{n} \frac{\widehat{\alpha}_k\{-[\alpha_T(T)\Omega]^2 + i\widehat{\phi}_k\alpha_T(T)\Omega\}}{-[\alpha_T(T)\Omega]^2 + i\widehat{\beta}_k\alpha_T(T)\Omega + \widehat{\delta}_k} \tag{38}$$

5 INFLUENCE OF MODEL PARAMETERS

The parameters of Eq. (14), for the fractional derivative model; of Eq. (27), for the standard GHM model; of Eq. (34), for the alternative GHM model; and of Eq. (36), for the modified GHM model can be related to typical features of the master curves. These features, shown in a pictorial fashion in Fig. (3), are the asymptotic behavior of the real modulus at lower and upper frequencies, the slope of the real modulus in the transition region, and the location of a fixed maximum loss factor.

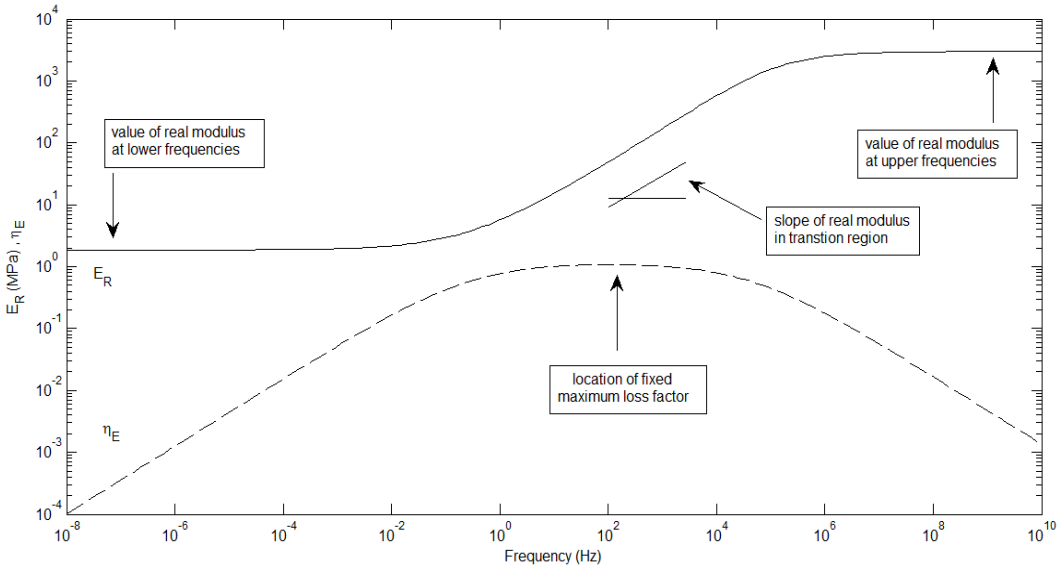

Figure 3: Typical features of dynamic property curves.

Such relationships highlight the influence of those parameters on the curves and can be accomplished by analyzing, in each case, the corresponding equation regarding the feature of concern (Bagley and Torvik, 1986; Lopes, 1998; Medeiros Jr. et al., 2011). Table 1 compiles the relevant features and the related model parameters, as far as the complex Young modulus is concerned. In that table, Ω_t is the transition frequency (Jones, 2001).

Table 1: Typical features and model parameters.

Feature	FD	SGHM	AGHM	MGHM
value of real modulus E_R at lower frequencies ($\Omega \to 0$)	E_0	E_C	E_∞, $\hat{\mu}$, $\hat{\delta}$	E_C
value of real modulus E_R at upper frequencies ($\Omega \to \infty$)	E_∞	E_C, $\hat{\alpha}$	E_∞	E_C, $\hat{\alpha}$
slope of real modulus E_R in transition region	β	E_C, $\hat{\alpha}$	$\hat{\mu}$, $\hat{\delta}$, $\hat{\theta}$	E_C, $\hat{\alpha}$
location of fixed maximum loss factor η_E (Ω_t)	b, β	$\hat{\beta}$, $\hat{\delta}$	$\hat{\beta}$, $\hat{\delta}$	$\hat{\beta}$, $\hat{\delta}$, $\hat{\phi}$

Parameter analyses can provide some directions regarding the search regions for the parameter values. The FD and the SGHM models have well defined search regions for their parameters. As for the AGHM model, it shows a broader search region than the SGHM model, while the MGHM model has a loosely defined search region, although it regains the control over the slope of the real modulus in the transition region, regarding the AGHM model. Furthermore, it is possible to verify that some parameter variations in the GHM models can cause abnormal behaviors on the dynamic curves (Medeiros Jr., 2010; Medeiros Jr. et al., 2011).

6 EXPERIMENTAL AND CURVE FITTING METHODS

In order to compare the adequacy of the above models, the dynamic properties were raised with the aid of a specific equipment called NETZSCH DMA 242 C. A typical viscoelastic material - commercially known as ISODAMP C-1002, manufactured by EAR Aearo Technologies LLC (3M Group) - was employed. Previous experiences in the characterization of viscoelastic materials, drawn from Jones (1992, 2001), Lopes (1998), Lopes et al. (2004), and Espíndola et al. (2005), led to the selection of 10 frequencies, namely: 0.1Hz, 0.2Hz, 0.5Hz, 1Hz, 2Hz, 5Hz, 10 Hz, 20 Hz, 50Hz, and 100Hz.

The temperatures were also chosen based on previous experiences, on the manufacturer's nomogram, and on preliminary tests of dynamic characterization performed with the complete experimental set-up. These temperatures, in a total of 7, were the following: -40 °C, -20 °C, -10 °C, 0 °C, 10 °C, 20 °C, and 50 °C. The smallest interval around 0 °C was due to the fact that the transition region of the material lies within that range. At each temperature, a prior 30 minute stabilization time was respected.

In order to avoid nonlinear effects, all measurements were made at low strain amplitudes. Fig. 4 shows a sample of viscoelastic material in the corresponding clamping device of the equipment, just above its thermal chamber. More details regarding the experiment can be found in Balbino et al. (2013).

Having obtained the experimental dynamic properties, the relative error to fit the models was defined as the difference between the experimental complex Young modulus ($\overline{E}_e$) and the predicted (computed) complex Young modulus ($\overline{E}$), divided by the absolute value of the experimental complex Young modulus ($\overline{E}_e$), such that

$$\overline{e}_{jk} = \left[\overline{E}_e(\Omega_j, T_k) - \overline{E}(\Omega_j, T_k)\right] / \left|\overline{E}_e(\Omega_j, T_k)\right| \tag{39}$$

where Ω_j was a given frequency, and T_k was a given temperature.



Figure 4: Experimental set-up.

The objective function *f(x)* for the curve fitting (minimization) process was the overall sum of the products of the relative errors by their corresponding complex conjugates, such that

$$f(x) = \sum_{k=1}^{q}\left[\sum_{j=1}^{p}\left(\overline{e}_{kj}\right)^{c}\left(\overline{e}_{jk}\right)\right] \tag{40}$$

where *p* and *q* were the number of frequencies and the number of temperatures, respectively.

As defined above, the objective function *f(x)* employs all the experimental complex Young modulus data (in both frequency and temperature) simultaneously in order to determine the model parameters of the viscoelastic material, including those parameters associated with the shift factor $\alpha_T(T)$ (Lopes et al., 2004). Thus, the necessary elements for a complete dynamic characterization of the material are obtained in a single procedure, from which the reduced frequency nomogram can be directly built.

The minimization was performed by the use of a hybrid strategy, which combined, in sequence, a genetic algorithm and a nonlinear optimization method, as implemented in the ga and fmincon proprietary MATLAB® routines, respectively. This choice proved to be particularly valuable when the GHM models were handled.

The design vectors for the FD, SGHM, AGHM and MGHM models were

$$x_{FD} = [E_0 \; E_\infty \; b \; \beta \; T_A] \tag{41}$$

$$x_{SGHM} = \left[E_C \; \hat{\alpha} \; \hat{\beta} \; \hat{\delta} T_A\right] \tag{42}$$

$$x_{AGHM} = \left[E_\infty \; \hat{\theta} \; \hat{\mu} \; \hat{\beta} \; \hat{\delta} \; T_A\right] \tag{43}$$

$$x_{MGHM} = \left[E_C \; \hat{\alpha} \; \hat{\phi} \; \hat{\beta} \; \hat{\delta} \; T_A\right] \tag{44}$$

as the Arrhenius equation (Eq. (8)) was chosen to model the shift factor $\alpha_T(T)$, in line with an observation made by Jones (1992) regarding the investigated viscoelastic material.

The MGHM model was also employed with one and two sets of additional parameters, denoted MGHM2 and MGHM3 models, respectively. The corresponding design vectors were

$$x_{MGHM2} = \left[E_c \; \hat{\alpha}_1 \; \hat{\phi}_1 \; \hat{\beta}_1 \; \hat{\delta}_1 \; \hat{\alpha}_2 \; \hat{\phi}_2 \; \hat{\beta}_2 \; \hat{\delta}_2 \; T_A\right] \tag{45}$$

$$x_{MGHM3} = \left[E_C \; \hat{\alpha}_1 \hat{\phi}_1 \; \hat{\beta}_1 \hat{\delta}_1 \; \hat{\alpha}_2 \; \hat{\phi}_2 \; \hat{\beta}_2 \; \hat{\delta}_2 \; \hat{\alpha}_3 \; \hat{\phi}_3 \hat{\beta}_3 \; \hat{\delta}_3 \; T_A \right] \tag{46}$$

Thus, the minimization problem was to find the design vector *x* for each model in order to minimize the objective function *f(x)*. Loose lower and upper bounds were also applied, based on the remarks made in section 5.

The curve fitting results were assessed in terms of the final values of the objective function and of those values divided by the number of degrees of freedom (the number of data points minus the number of fitted parameters) (Motulsky and Ransnas, 1987). Plots of experimental-predicted real Young modulus data and of the corresponding relative residuals were also generated, since the real Young modulus is a key dynamic property when calculating the stiffness of vibration isolators and dynamic neutralizers (Espíndola et al., 2010). The relative residuals were computed as the difference between the experimental and the predicted real modulus over the experimental modulus.

The Akaike's Information Criterion (AIC) was also employed in the analysis. Although not widely known, the AIC proved to be a very valuable and consistent tool. Its theoretical basis can be found in Burnham and Anderson (2002). The main concepts and equations - with the corresponding interpretation - are summarized below, following the lines of Motulsky and Christopoulos (2003).

The AIC is defined by

$$AIC = N.\ln\left(\frac{SS}{N}\right) + 2K \tag{47}$$

where N is the number of data points, SS is the sum of squares (given, in that case, by the value of the objective function), and K is the number of fitted parameters plus one

As pointed out by Motulsky and Christopoulos (2003), the AIC takes into account the sum of squares and the number of fitted parameters in evaluating the goodness-of-fit. It is also highlighted that the value of the AIC lies in comparing models, so that what really matters is the difference between AIC values of models of concern. The individual AIC values are computed and the model with the smallest AIC value is the most likely to be correct.

Given its better adequacy, it is recommended that the second-order (corrected) AIC values should always be used. It is calculated by

$$AIC_C = AIC + \frac{2K\left(K+1\right)}{N-K-1} \tag{48}$$

and its use is the same as that explained above.

When two particular models A and B are compared in terms of their AICc values, the probability Pr of choosing the correct model is computed by

$$Pr = \frac{e^{-0.5\Delta}}{1+e^{-0.5\Delta}} \tag{49}$$

where Δ is the difference between AICc values (smaller minus greater). It can then be stated that there is a (Pr x 100%) probability that model A is correct, and a [(1 – Pr) x 100%] probability that model B is correct.

Taking the above definitions into account, the probability that one model is correct can be divided by the probability the other model is correct in order to give a quantity called evidence ratio (ER). It is given by

$$ER = e^{-0.5\Delta} \tag{50}$$

and allows one to state, within the limits of the corresponding experimental design, that one model is (ER) times more likely to be correct than the other model.

7 RESULTS

The results of the current investigation are presented in this section with the corresponding comments.

Figure 5 displays the wicket plot for the experimental data. As shown by Jones (1992, 2001), adequate experimental data should form an “inverted” U curve in a wicket plot, which is satisfactorily seen in that figure.

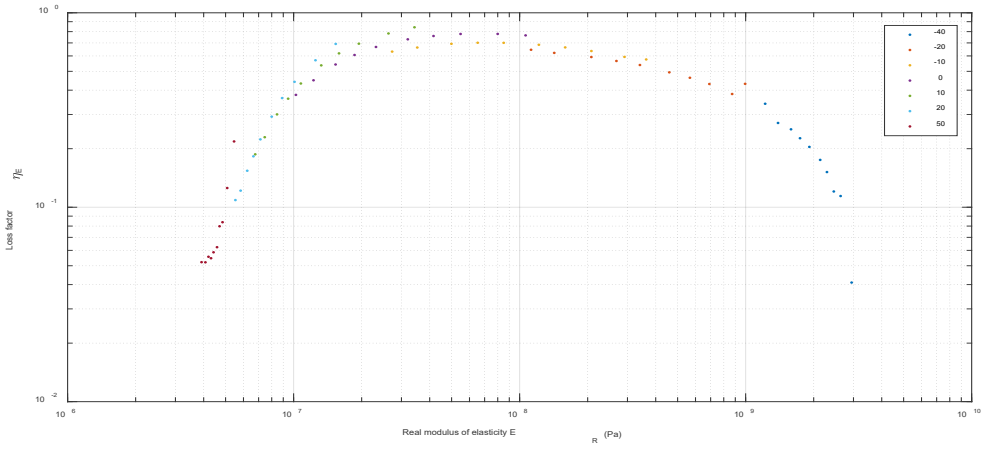

Figure 5: Wicket plot of experimental data.

Table 2 presents the final values of the objective function for all the investigated models, along with those values divided by the number of degrees of freedom (number of data points minus number of fitted parameters). It can be observed that the FD model shows the lowest values. The values for the MGHM model are lower than the corresponding values for the SGHM and the AGHM models. When sets of additional terms are considered in the MGHM model, the values decrease progressively.

Table 2: Final values of the objective function.

	FD	SGHM	AGHM	MGHM	MGHM2	MGHM3
final f(x)	0.497	22.8	22.8	11.8	5.80	3.13
final f(x)/df	0.0875	0.592	0.597	0.430	0.311	0.237

Tables 3 to 8 contain the values of the fitted parameters, regarding the investigated models.

Table 3: Parameter values – FD model.

$E_0 = 4.42x10^6\,Pa$	$E_\infty = 2.54x10^9\,Pa$	$b = 3.80x10^{-3}\,s^\beta$	$\beta = 4.11x10^{-1}$	$T_A = 9.74x10^3\,K$

Table 4: Parameter values – SGHM model.

$E_C = 5.89x10^6\,Pa$	$\hat{\alpha} = 2.55x10^8\,Pa$	$\hat{\beta} = 7.41x10^7\,s^{-1}$	$\hat{\delta} = 2.80x10^{10}\,s^{-2}$	$T_A = 8.06x10^3\,K$

Table 5: Parameter values – AGHM model.

$E_\infty = 8.17x10^7\,Pa$	$\hat{\theta} = 4.43x10^{17}\,Pa.s^{-}$	$\hat{\mu} = -7.03x10^{19}\,Pa.s^{-}$	$\hat{\beta} = 2.49x10^9\,s^{-}$	$\hat{\delta} = 9.27x10^{11}\,s^{-}$ $T_A = 8.12x10^3\,K$

Table 6: Parameter values – MGHM model.

$E_c = 5.76x10^6\,Pa$	$\hat{\alpha} = 1.27x10^9\,Pa$	$\hat{\phi} = 1.39x10^3\,s^{-1}$	$\hat{\beta} = 1.93x10^4\,s^{-1}$	$\hat{\delta} = 1.10x10^6\,s^{-2}$	$T_A = 8.12x10^3\,K$

Table 7: Parameter values – MGHM2 model (one set of additional parameters).

$E_C = 5.38x10^6\,Pa$	$\hat{\alpha}_1 = 1.57x10^9\,Pa$	$\hat{\phi}_1 = 1.03x10^3\,s^{-1}$	$\hat{\beta} = 7.57x10^4\,s^{-1}$	$\hat{\delta} = 2.62x10^5\,s^{-2}$
$T_A = 8.76x10^3\,K$	$\hat{\alpha}_2 = 6.77x10^5\,Pa$	$\hat{\phi}_2 = 2.18x10^7\,s^{-1}$	$\hat{\beta}_2 = 7.62x10^4\,s^{-1}$	$\hat{\delta}_2 = 3.31x10^7\,s^{-2}$

Table 8: Parameter values – MGHM3 model (two sets of additional parameters).

$E_c = 5.07x10^6\,Pa$	$\hat{\alpha}_1 = 1.84x10^9\,Pa$	$\hat{\phi}_1 = 9.60x10^3\,s^{-1}$	$\hat{\beta}_1 = 2.94x10^5\,s^{-1}$	$\hat{\delta}_1 = 1.44x10^7\,s^{-2}$
$T_A = 9.16x10^3\,K$	$\hat{\alpha}_2 = 3.93x10^5\,Pa$	$\hat{\phi}_2 = 2.50x10^8\,s^{-1}$	$\hat{\beta}_2 = 2.97x10^5\,s^{-1}$	$\hat{\delta}_2 = 7.09x10^8\,s^{-2}$
	$\hat{\alpha}_3 = 5.45x10^7\,Pa$	$\hat{\phi}_3 = 3.77x10^{10}\,s^{-1}$	$\hat{\beta}_3 = 2.09x10^{11}\,s^{-1}$	$\hat{\delta}_3 = 1.15x10^{11}\,s^{-2}$

Figures 6 to 11 portrait the plots of experimental-predicted real Young modulus data. As pointed out previously, the real modulus is a key dynamic property for designing viscoelastic devices for vibration control. It can be visually observed that the FD model is clearly the best in fitting the experimental data, when compared to the SGHM, the AGHM, and the MGHM models. When additional terms are included in the MGHM model, the corresponding plots show progressive improvement (as possibly expected), but the FD model still seems to be the best.

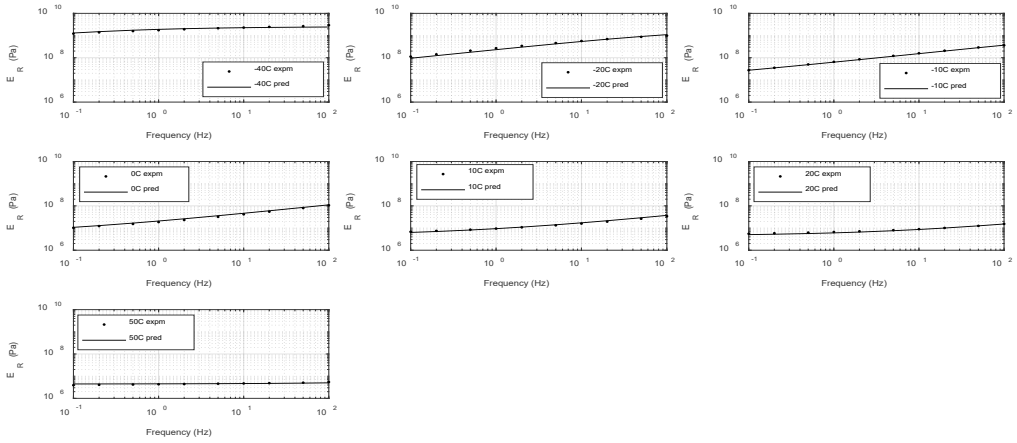

Figure 6: Experimental-predicted real modulus data – FD model.

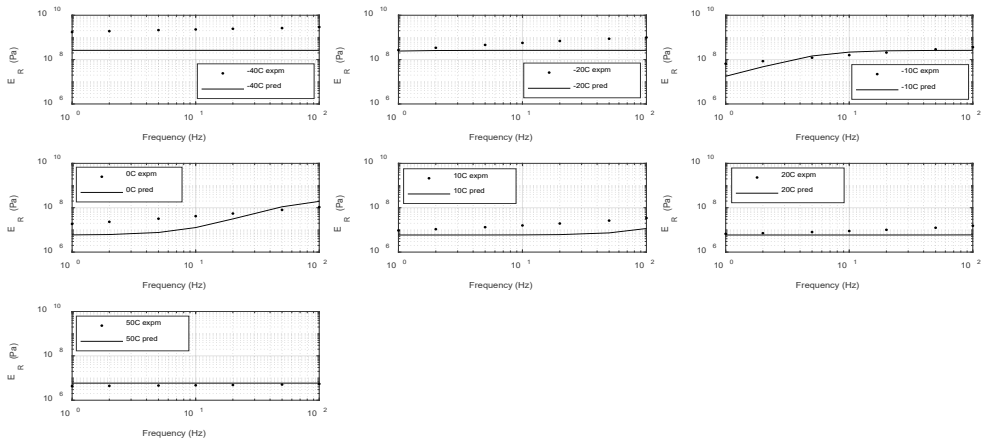

Figure 7: Experimental-predicted real modulus data – SGHM model.

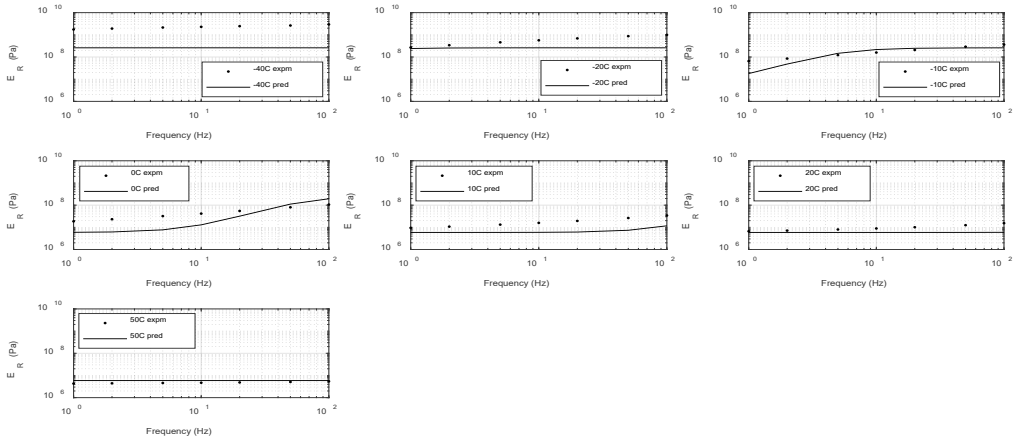

Figure 8: Experimental-predicted real modulus data – AGHM model.

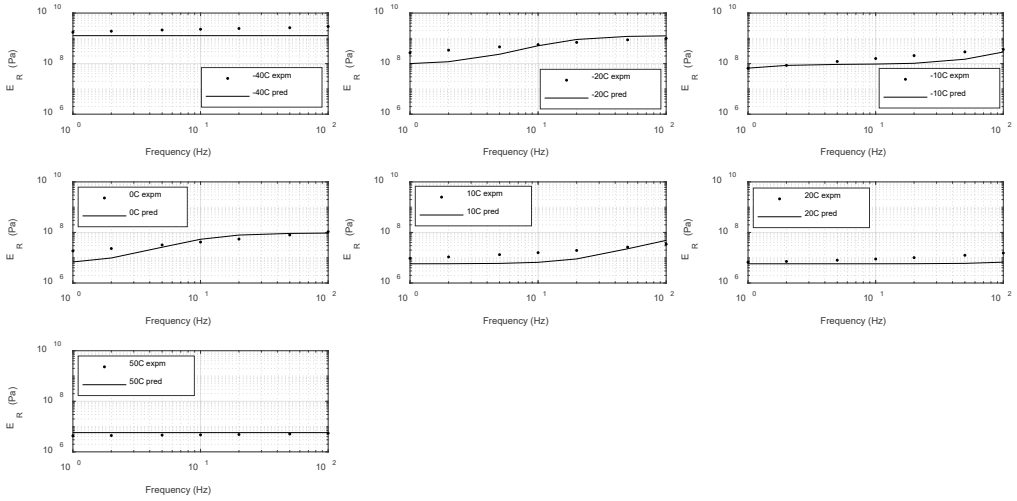

Figure 9: Experimental-predicted real modulus data – MGHM model.

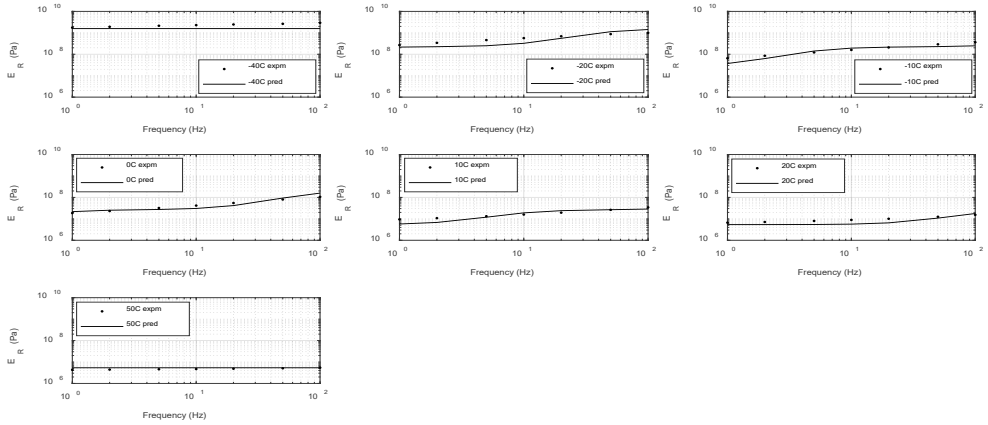

Figure 10: Experimental-predicted real modulus data – MGHM2 model.

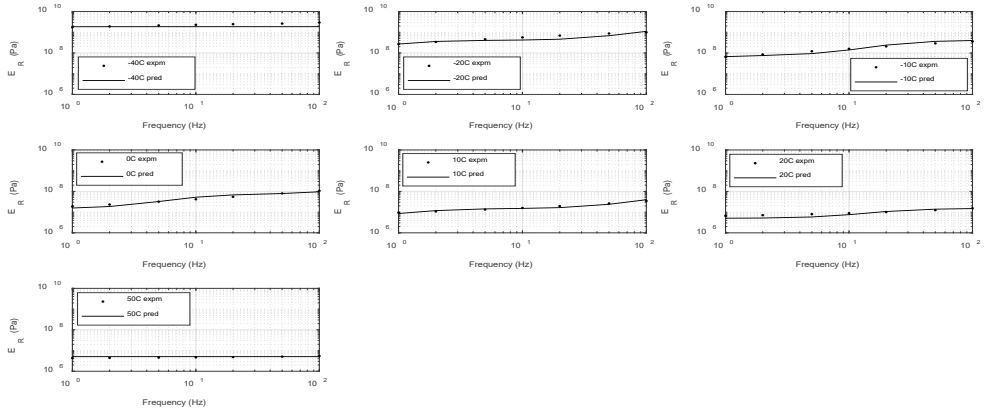

Figure 11: Experimental-predicted real modulus data – MGHM3 model.

Figures 12 to 17 show the associated plots of relative residuals (each relative residual is the difference between the experimental and the predicted values over the experimental value), whereas the histograms for these relative residuals, regarding their relative frequencies, are displayed in Fig. 18. It can be observed that there is a general trend for the SGHM, the AGHM, and the MGHM models to underestimate the real Young modulus. As additional terms are included in the MGHM model, the relative residuals become more balanced, such as the case of the FD model.

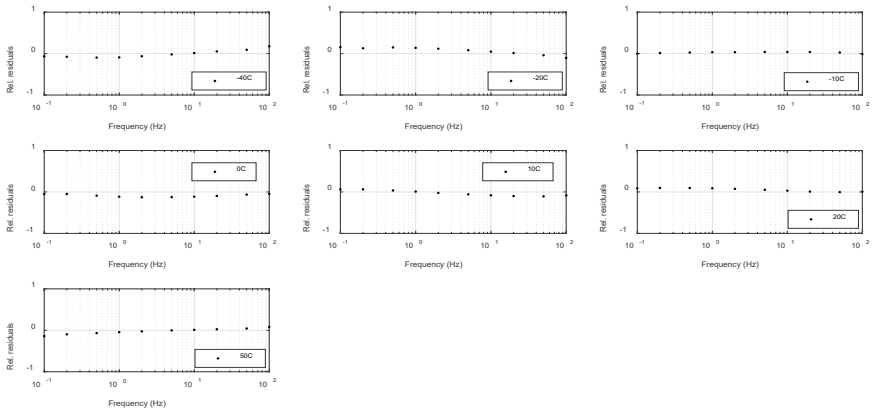

Figure 12: Relative residuals for real modulus data – FD model.

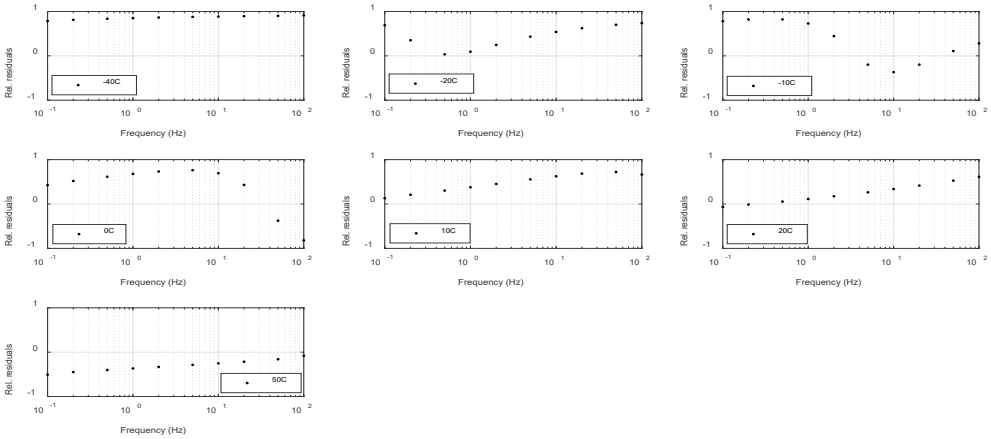

Figure 13: Relative residuals for real modulus data – SGHM model.

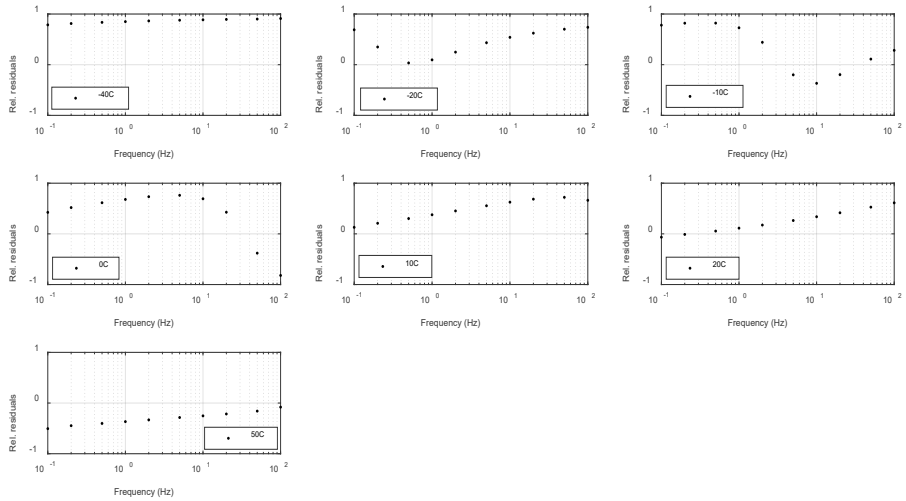

Figure 14: Relative residuals for real modulus data – AGHM model.

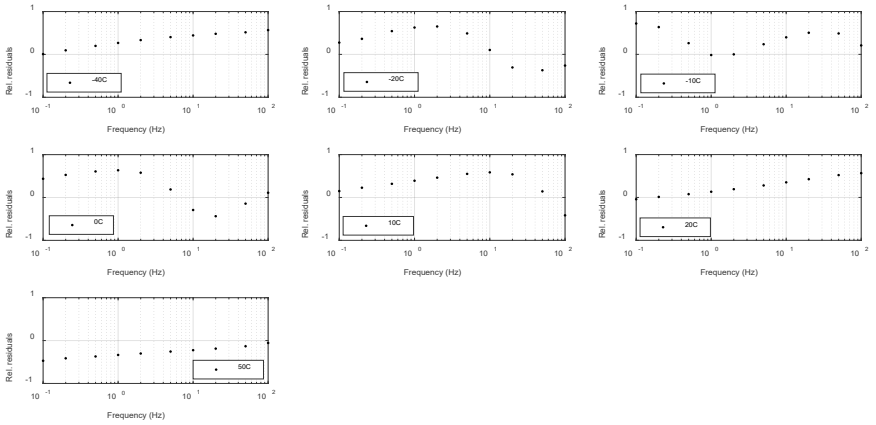

Figure 15: Relative residuals for real modulus data – MGHM model.

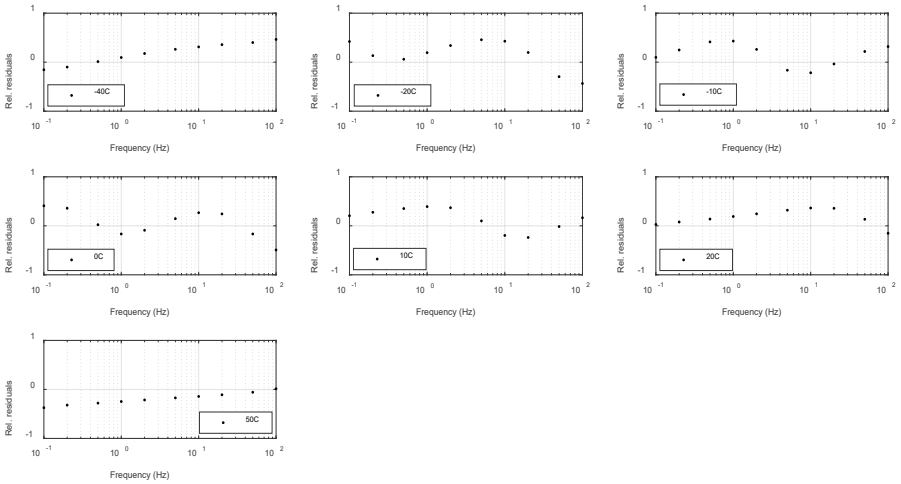

Figure 16: Relative residuals for real modulus data – MGHM2 model.

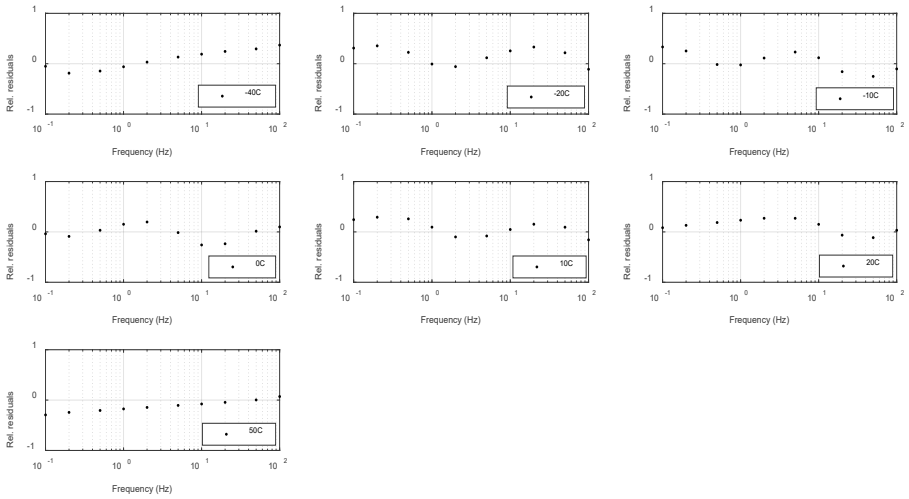

Figure 17: Relative residuals for real modulus data – MGHM3 model.

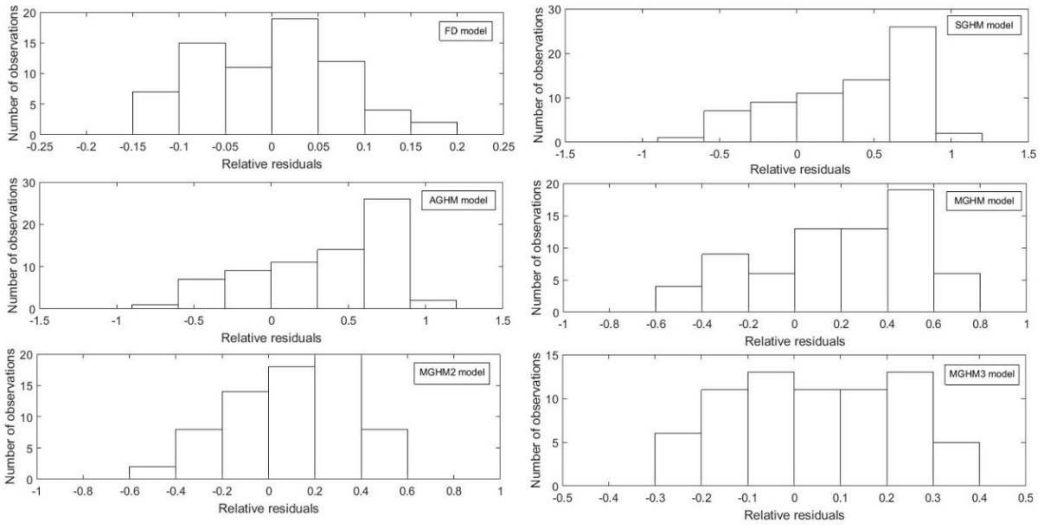

Figure 18: Histograms of relative residuals for real modulus data.

Table 9 contains the AICc values for the models of concern. It is observed that the FD model has the lowest value among all the models and that, when compared to the SGHM and the AGHM models, the MGHM model has the lowest value. As additional terms are considered in the MGHM model, the AICc value becomes progressively lower. These observations are fully in line with the results in Table 2 and Figs. 6 to 11.

Table 9: AICc values.

	FD	SGHM	AGHM	MGHM	MGHM2	MGHM3
AICc	-333.0	-65.26	-62.79	-108.7	-147.8	-178.5

As for the probabilities, they are displayed in Table 10, in which each model on the left is compared to a distinct model on the top. From these results, which follow from those in Table 9, it can be stated that the FD model is the most likely to be correct, with 100% probability in all the pertinent comparisons. The MGHM model, on its turn, is more likely to be correct than the SGHM and the AGHM models, also with 100% probability.

As additional terms are included in the MGHM model, a progressive improvement is clearly observed. In fact, it can be stated that, in the context of a wide frequency and temperature dynamic characterization, not only is the inclusion of additional terms desirable but highly recommended.

Table 10: Comparative probabilities.

	FD	SGHM	AGHM	MGHM	MGHM2	MGHM3
FD	-----	100%	100%	100%	100%	100%
SGHM	0%	-----	77.5%	0%	0%	0%
AGHM	0%	22.5%	-----	0%	0%	0%
MGHM	0%	100%	100%	-----	0%	0%
MGHM2	0%	100%	100%	100%	-----	0%
MGHM3	0%	100%	100%	100%	100%	-----

8 CONCLUSIONS

A comparative study involving fractional derivative and GHM models was performed, regarding a broad dynamic characterization of a typical viscoelastic material, in terms of both frequency and temperature. Distinctive use of the Akaike's Information Criterion was made.

For a wide frequency and temperature representation of the viscoelastic material, it is shown that the fractional derivative model is the most likely to be correct. It stands out even when additional terms are considered in the MGHM model, which is the most likely to be correct among its counterparts. Additional terms are highly recommended when the MGHM is to be employed in the current context.

REFERENCES

Bagley, R. L. and Torvik, P. J., (1983). A Theoretical Basis for the Application of Fractional Calculus to Viscoelasticity. Journal of Rheology. Vol. 27, pp. 201–210.

Bagley, R. L. and Torvik, P. J., (1986). On the Fractional Calculus Model of Viscoelastic Behaviour. Journal of Rheology. Vol. 30, pp. 133–155.

Bagley, R. L., (1979). Applications of Generalized Derivatives to Viscoelasticity. Doctor of Philosophy Dissertation, Faculty of the School of Engineering of the Air Force Institute of Technology. Defense Technical Information Center, document AD-A071726.

Balbino, F. O., Munaro, M., Lopes, E. M. O., (2013). Statistical Analysis of Experimental Data in Dynamic Characterization of Viscoelastic Materials. Proceedings of the XXXIV Iberian Latin-American Congress on Computational Methods in Engineering, Pirenópolis (GO), Brazil.

Barbosa, F. S. and Farage, M. C. R., (2008). A finite element model for sandwich viscoelastic beams: Experimental and numerical assessment. Journal of Sound and Vibration. Vol. 317(1-2), pp. 91–111.

Barbosa, F. S., (2000). Modelagem Computacional de Estruturas com Camadas Viscoelásticas Amortecidas. Tese de Doutorado. Universidade Federal do Rio de Janeiro (in Portuguese).

Biot, M. A., (1955). Variational Principles in Irreversible Thermodynamics with Application to Viscoelasticity. Physical Review. Vol. 97(6), pp. 1463–1469.

Burnham, K. P., Anderson, D. R., (2002). Model Selection and Multimodal Inference – A Practical Information-Theoretic Approach, 2nd. ed., Springer.

Christensen, R.M., (1982). Theory of Viscoelasticity – An Introduction, 2nd. ed., Academic Press.

Cinielo, A. P. D., Bavastri, C. A., Pereira, J. T., (2017). Identifying Mechanical Properties of Viscoelastic Materials in Time Domain using the Fractional Zener Model. Latin American Journal of Solids and Structures. Vol. 14, pp. 131-152.

Cunha-Filho, A. G., Lima, A. M. G., Donadon, M. V., Leão, L. S., (2016). Flutter Suppression of Plates Subjected to Supersonic Flow Using Passive Constrained Viscoelastic Layers and Golla-Hughes-McTavish Method. Aerospace Science and Technology. Vol. 52, pp. 70-80.

Espíndola, J. J., Bavastri, C. A., Lopes, E. M. O, (2010). On the passive control of vibrations with viscoelastic dynamic absorbers of ordinary and pendulum types. Journal of the Franklin Institute. Vol. 347, pp. 102–115.

Espíndola, J. J., Lopes, E. M. O., Silva Neto, J. M., (2005). A Generalised Fractional Derivative Approach to Viscoelastic Material Properties Measurement. Applied Mathematics and Computation. Vol. 164(2), pp.493–506.

Friswell, M. I., Inman, D. J., Lam, M. J., (1997). On the Realisation of GHM Models in Viscoelasticity. Journal of Intelligent Material Systems and Structures. Vol. 8(11), pp. 986–993.

Gibson, W.C. and McTavish, D.J., (1995). Implementation of the GHM Method for Viscoelastic Material using Matlab and Nastran. Proceedings of SPIE. Vol. 2445, pp. 312-323.

Golla, D.F. and Hughes, P.C., (1985). Dynamic of Viscoelastic Structures – A Time Domain, Finite Element Formulation. Journal of Applied Mechanics. Vol. 52, pp. 897–905.

Jones, D.I.G., (1992). Results of a Round Robin Test Program: Complex Modulus Properties of a Polymeric Damping Material. Final Report no. WL-TR-92-3104. Wright-Patterson Air Force Base, Ohio, USA.

Jones, D.I.G., (2001). Handbook of Viscoelastic Vibration, John Wiley & Sons.

Katsikadelis, J. T., (2015). Generalized fractional derivatives and their applications to mechanical systems. Archive of Applied Mechanics. Vol. 85, pp. 1307-1320.

Kattimani, S. C. and Ray, M. C., (2014). Smart Damping of Geometrically Nonlinear Vibrations of Magneto-Electro-Elastic Plates. Composite Structures. Vol. 114, pp. 51-63.

Kattimani, S. C. and Ray, M. C., (2015). Control of Geometrically Nonlinear Vibrations of Functionally Graded Magneto-Electro-Elastic Plates. International Journal of Mechanical Sciences. Vol. 99, pp. 154-167.

Lopes, E.M.O., (1998). On the Experimental Response Reanalysis of Structures with Elastomeric Materials, PhD Thesis. University of Wales Cardiff.

Lopes, E.M.O., Bavastri, C.A., Espíndola, J.J., Silva Neto, J.M., (2004). Caracterização Dinâmica Integrada de Elastômeros por Derivadas Generalizadas. Anais do III Congresso Nacional de Engenharia Mecânica (in Portuguese).

Mainardi, F., (2010). Fractional Calculus and Waves in Linear Viscoelasticity. Imperial College Press.

Martin, L. A. and Inman, D. J., (2013). A Novel Viscoelastic Material Modulus Function for Modifying the Golla-Hughes-McTavish Method. International Journal of Acoustics and Vibration. Vol. 18(3), pp. 102-108.

Martin, L.A., (2011). A Novel Material Modulus Function for Modeling Viscoelastic Materials, PhD Dissertation, Virginia Polytechnic Institute and State University.

Mead, D. J., (2000). Passive Vibration Control, John Wiley & Sons.

Medeiros Jr, W. B., (2010). Caracterização Dinâmica Integrada de Elastômeros via Derivadas Fracionárias e Método GHM. Dissertação de Mestrado, Universidade Federal do Paraná (in Portuguese).

Medeiros Jr, W. B., Espíndola, J. J., Bavastri, C. A., Lopes, E. M. O., (2011). Integrated Dynamic Characterization of Viscoelastic Materials by Fractional Derivative and GHM Models, Proceedings of the XXXII CILAMCE, Ouro Preto (MG), Brazil.

Moschen, I.C., (2006). Sobre as Funções Mittag-Leffler e o Modelo Fracionário de Materiais Viscoelásticos. Tese de Doutorado. Universidade Federal de Santa Catarina (in Portuguese).

Motulsky, H. J., Christopoulos, A. (2003). Fitting Models to Biological Data using Linear and Nonlinear Regression – A Practical Guide to Curve Fitting. GraphPad Software Inc., San Diego CA, www.graphpad.com .

Motulsky, H. J., Ransnas, L. A., (1987). Fitting Curves to Data using Nonlinear Regression: a Practical and Nonmathematical Review. FASEB Journal. Vol. 1, pp. 365-374.

Nashif, A. D., Jones, D.I.G., Henderson, J.P., (1985). Vibration Damping, John Willey & Sons.

Papoulis, A., (1962). The Fourier Integral and its Applications, McGraw-Hill.

Pritz, T., (1996). Analysis of Four-Parameter Fractional Derivative Model of Real Solid Materials. Journal of Sound and Vibration. Vol. 195(1), pp. 103–115.

Pritz, T., (1998). Frequency Dependences of Complex Moduli and Complex Poisson's Ratio of Real Solid Materials. Journal of Sound and Vibration. Vol. 214(1), pp. 83–104.

Pritz, T., (2003). Five-Parameter Fractional Derivative Model for Polymeric Damping Materials. Journal of Sound and Vibration. Vol. 265, pp. 935-952.

Ribeiro, E. A., Pereira, J. T., Bavastri, C. A., (2015). Passive Vibration Control in Rotor Dynamics: Optimization of Composed Support Using Viscoelastic Materials. Journal of Sound and Vibration. Vol. 351, pp. 43-56.

Snowdon, J.C., (1968). Vibration and Shock in Damped Mechanical Systems, John Wiley & Sons.

Sun, L. and Chen, L., (2015). Free Vibrations of a Taut Cable with a General Viscoelastic Damper Modeled by Fractional Derivatives. Journal of Sound and Vibration. Vol. 335, pp. 19-33.

Zghal, S., Bouazizi, M. L., Bouhaddi, N., Nasri, R., (2015). Model Reduction Methods for Viscoelastic Sandwich Structures in Frequency and Time Domains. Finite Elements in Analysis and Design. Vol. 93, pp. 12-29.

Zhu, S., Cai, C., Snapos, P. D., (2015). A Nonlinear and Fractional Derivative Viscoelastic Model for Rail Pads in the Dynamic Analysis of Coupled Vehicle-Slab Track Systems. Journal of Sound and Vibration. Vol. 335, pp. 304-320.